



Citation for published version:

El-Bana, MS, Wolverson, D, Russo, S, Balakrishnan, G, Paul, DM & Bending, SJ 2013, 'Superconductivity in two-dimensional NbSe₂ field effect transistors', *Superconductor Science and Technology*, vol. 26, no. 12, 125020, pp. 26. <https://doi.org/10.1088/0953-2048/26/12/125020>

DOI:

[10.1088/0953-2048/26/12/125020](https://doi.org/10.1088/0953-2048/26/12/125020)

Publication date:

2013

Document Version

Peer reviewed version

[Link to publication](#)

University of Bath

Alternative formats

If you require this document in an alternative format, please contact:
openaccess@bath.ac.uk

General rights

Copyright and moral rights for the publications made accessible in the public portal are retained by the authors and/or other copyright owners and it is a condition of accessing publications that users recognise and abide by the legal requirements associated with these rights.

Take down policy

If you believe that this document breaches copyright please contact us providing details, and we will remove access to the work immediately and investigate your claim.

Superconductivity in two-dimensional NbSe₂ Field Effect Transistors

Mohammed S El-Bana^{1,2}, Daniel Wolverson¹, Saverio Russo³ and Simon J Bending¹

¹Department of Physics, University of Bath, Claverton Down, Bath BA2 7AY, UK

²Department of Physics, Faculty of Education, Ain Shams University, Cairo, Egypt

³Physics, College of Eng., Math. & Phys. Sciences, University of Exeter, Exeter EX4 4QL, UK

Abstract

We describe investigations of superconductivity in few molecular layer NbSe₂ field effect transistors. While devices fabricated from NbSe₂ flakes less than 8 molecular layers thick did not conduct, thicker flakes were superconducting with an onset T_c that was only slightly depressed from the bulk value for 2H-NbSe₂ (7.2K). The resistance typically showed a small, sharp high temperature transition followed by one or more broader transitions which usually ended in a wide tail to zero resistance at low temperatures. We speculate that these multiple resistive transitions are related to disorder in the layer stacking. The behavior of several flakes has been characterized as a function of temperature, applied field and back-gate voltage. We find that the conductance in the normal state and transition temperature depend weakly on the gate voltage, with both conductivity and T_c *decreasing* as the electron concentration is *increased*. The application of a perpendicular magnetic field allows the evolution of different resistive transitions to be tracked and values of the zero temperature upper critical field, $H_{c2}(0)$, and coherence length, $\xi(0)$, to be independently estimated. Our results are analyzed in terms of available theories for these phenomena.

Keywords

NbSe₂, 2D superconductivity, Field effect transistors

1. Introduction

The first isolation of graphene in 2004 [1] has led to a resurgence of interest in the study of layered materials. In particular it has been shown that these can form the basis of truly two-dimensional atomic crystals with remarkable electronic properties and very high specific surface areas, making them suited for applications ranging from electronic devices to energy storage [2]. The physical insights obtained from working with graphene, as well as a requirement for other 2D materials with complementary electronic properties, has directed attention towards studies of atomically thin forms of

the transition metal dichalcogenides (TMDs). These are very promising candidates for nanoscale applications as they exhibit a rich variety of electronic ground states (e.g., metallic, semiconductor, superconductor, and charge density wave (CDW)) [3]. One of the more interesting TMDs is the quasi two-dimensional superconductor niobium diselenide. This has two common hexagonal crystalline forms with slightly different bulk critical temperatures, 2H-NbSe₂ and 4H-NbSe₂, where the numerical prefix indicates the number of NbSe₂ molecules in the unit cell. The 2H-NbSe₂ unit cell of interest here contains two NbSe₂ molecular layers in AB stacking. Each molecular unit is formed from a sandwich of two layers of Se atoms with a plane of Nb atoms between them, and the coordination numbers of the Se and Nb atoms are 3 and 6 respectively. The lattice constants of 2H-NbSe₂ are $a=b=3.6 \text{ \AA}$ and $c=12.6 \text{ \AA}$, and the spacing between adjacent Nb sheets is hence 6.3 \AA [4]. NbSe₂ molecular layers are strongly covalently bonded while there is only a weak van der Waals interaction between adjacent layers [5, 6]. Consequently, it is easy to cleave 2H-NbSe₂ sheets along planes parallel to the a-b face and the terminating surface after exfoliation is usually a Se layer [7]. 2H-NbSe₂ is metallic at high temperatures but becomes a type II superconductor below a critical temperature of $T_c \approx 7.2 \text{ K}$. This material is believed to be a conventional s-wave superconductor, albeit a highly anisotropic one, and in high quality samples superconductivity coexists with a charge density wave (CDW) [which sets in](#) below $T \sim 32 \text{ K}$. To date there has been little agreement on the nature of the competition between these two ground states [8].

Frindt [7] published the first investigations of few molecular layer 2H-NbSe₂ flakes mechanically exfoliated onto various substrates. He observed a decrease in T_c with decreasing flake thickness, a trend that became particularly pronounced in samples estimated to be less than six molecular layers thick. This author was not able to measure flake thicknesses directly but inferred them from the 300 K resistances assuming an effective bulk resistivity of $160 \mu\Omega\cdot\text{cm}$. Using this thickness calibration, the T_c of a single molecular layer was predicted to be 3.8 K (c.f., $T_c = 7.2 \text{ K}$ in bulk samples). Multiple steps observed in the resistive superconducting transition were associated with regions of the flakes with different thicknesses.

More recently Novoselov *et al.* [9] reported measurements of field effect transistors fabricated from single molecular layers of NbSe₂ mechanically exfoliated onto Si/SiO₂ substrates. They observed semi-metallic behaviour at 300K with an electron concentration that was two orders of magnitude smaller than that expected from scaling bulk values, suggesting significant changes in the electronic energy spectrum. The dynamic 'field-effect' mobility of their devices was measured to be in the range $0.5\text{-}3 \text{ cm}^2/\text{Vs}$, with an *increase* in conductivity as the electron concentration was increased.

In the most recent study of atomically thin NbSe₂ flakes Staley *et al.* [5] have realised two-terminal field effect transistors fabricated by mechanical exfoliation onto Si/SiO₂ substrates followed by a lithography-free shadow masking contact process. These authors observed superconductivity in devices which were only single unit cells (two molecular layers) thick with T_c as high as 2.5 K . They

measured the dynamic mobility for their samples to be in the range $\sim 10\text{-}60\text{ cm}^2/\text{Vs}$ and observed a clear modulation of T_c with gate voltage in the thinnest flakes. This was interpreted in terms of a simple model for changes in the electronic density of states, but did not address the fact that T_c decreases with increasing electron density.

The motivation for this paper is to extend these studies of the field effect on superconductivity in NbSe₂ flakes to lithographically-defined 4-terminal structures in which the number and quality of molecular layers has been fully characterised. It is now well-established that the modulation of the charge carrier density in a superconductor can change its physical properties, in particular the superconducting transition temperature, T_c . Several conditions must be satisfied in order to observe a measurable electric field effect on superconductivity. Since the carrier density of most metallic superconducting materials is high, a very thin layer of material is needed in order to be able to achieve significant charge density modulation. In addition, a high-quality dielectric is important in order to enhance the electric field and allow high gate voltages to be applied. Finally, a good control of material interfaces is crucial in order that the behaviour of the device is not undesirably limited by charge redistribution at the flake/substrate and flake/dielectric interfaces rather than changes in the chemical potential of the superconducting flake itself [5]. In our experiments most of these criteria are well satisfied, allowing us to make systematic studies of the electrical properties of thin NbSe₂ flakes as a function of temperature, perpendicular magnetic field and back gate voltage.

2. Experimental Method

Our four-terminal field-effect devices were fabricated using micromechanical cleavage of high quality 2H-NbSe₂ single crystals onto Si/SiO₂ substrates. Optimisation of this process using pairs of permanent magnets to apply a controlled pressure allowed flakes up to $\sim 70\text{ }\mu\text{m}$ in size to be exfoliated (c.f., figure 1(a)). Substrates were etched in piranha solution prior to exfoliation in order to remove any organic residues from the surface. Highly doped Si substrates with a 297 nm SiO₂ top layer were used as this was found to give good optical contrast for deposited NbSe₂ flakes under the microscope. The SiO₂ layer also acts as a robust dielectric allowing the Si substrate to be used as a ‘back gate’ up to relatively high voltages ($\sim \pm 100\text{V}$). Atomic force microscopy and Raman spectroscopy were used to characterise the quality and number of molecular layers present in our flakes.

Two levels of Electron Beam Lithography (EBL) were used to define both the inner electrodes (Cr/Au 10/50 nm) and outer bond pads (Cr/Au 20/250 nm) in PMMA, followed by electron-beam deposition of Cr/Au films and lift-off in acetone. In both EBL steps patterns were aligned to markers defined on the Si/SiO₂ wafer by optical lithography prior to exfoliation. The lateral width of electrodes varied from 1-1.5 μm with the spacing between electrodes ranging from 1 to 3 μm , (c.f., figure 1(b,c)). A schematic diagram of a completed NbSe₂ field effect transistor is shown in figure 1(d).

Completed devices were wire-bonded in a DIL ceramic package and mounted on a temperature-controlled sample holder which was coupled to a liquid Helium bath via exchange gas. Small signal magneto-transport measurements were performed in a variable temperature Helium cryostat with a base temperature of 2.0 K. Great care was taken to avoid damage to devices arising from electrostatic shock, and all leads down to the sample were protected with custom-designed pi filters. Four-point measurements were performed with a constant $1 \mu\text{A}$ 32Hz ac current, and voltages were detected using a digital lock-in amplifier. Magnetic fields up to 1T could be applied perpendicular to the NbSe₂ flakes with a small superconducting solenoid in the liquid Helium bath.

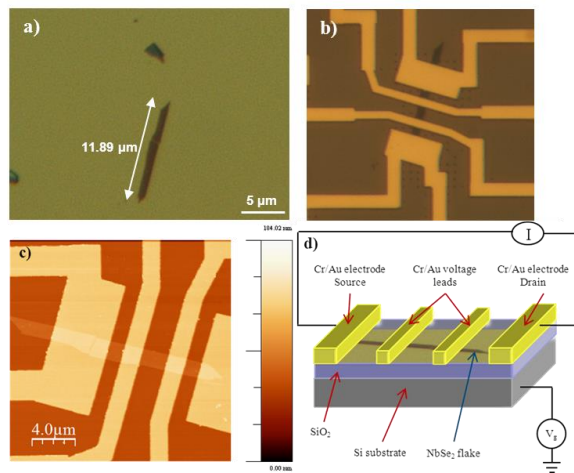


Figure 1. (Colour online) Optical micrographs of the exfoliated flake (a) and the completed device (b). (c) Topographic AFM image for the 7.92 nm thick flake device. (d) Schematic representation of a NbSe₂ FET.

3. Results

3.1 Flake characterization

Several complementary techniques were used to characterize the flakes in our NbSe₂ FETs. Single and few-layer flakes were readily recognized under an optical microscope; different thickness flakes have distinct interference colors with white light illumination. Many of these flakes clearly had regions containing different numbers of molecular layers and only homogeneous ones were selected for device fabrication. Tapping mode Atomic Force Microscopy (AFM) was used to quantitatively measure the thicknesses of NbSe₂ flakes (and contacts) on Si/SiO₂ substrates after low temperature electrical measurements had been completed. Although, as is well known for graphene, such AFM estimates could contain systematic errors, samples will henceforth be referred to by these nominal AFM

thicknesses which are listed in table 1. AFM was also used to determine the lateral flake dimensions given in this table.

Raman spectroscopy was used to characterize further all of the samples studied. NbSe₂ flakes were studied at room temperature under a Renishaw inVia Raman Microscope operating at a 532 nm excitation wavelength. A short working distance 50x objective lens was used to capture Raman spectra from samples with integration times in the range 100-400 s. Figure 2 shows Raman spectra for a selection of flakes of different thicknesses that have all been captured with a laser power of 0.05 mW and an integration time of 100 s. In the thickest samples the out-of-plane phonon mode A_{1g} (228 cm⁻¹), and the in-plane phonon mode E_{2g} (237 cm⁻¹) were well resolved in the Raman spectra. However, decreasing flake thickness tended to be accompanied by a broadening of the two phonon peaks, resulting in almost complete overlap in the thinnest flakes as seen in figure 2. We observe an apparently non-monotonic shift of both phonon modes as the flake thickness is reduced, in agreement with the results of Staley *et al.* [5, 10]. Hence this shift cannot easily be used to characterize the layer number in NbSe₂ in contrast to the situation in few-layer graphene [5] and we propose an explanation for this shift as follows.

Spectra obtained with high laser intensity or long laser exposures were found to evolve with time, and AFM scans revealed that flakes actually thickened after laser exposure. This suggests that structural changes have occurred, of which the most likely are decomposition to produce Se precipitates, or oxidation; in addition, it is known that photo-oxidation of NbSe₂ leads to an increase in volume [11]. To resolve this question, we show in Figure 3 a series of Raman spectra for a 6.56 nm flake as a function of laser power. These clearly show the appearance of a new peak near 302 cm⁻¹ at high powers (and long times); we note that this peak is also evident in figure 2 of Staley *et al.* [5], who also comment that laser-induced damage was found for thin flakes. By reference to earlier studies of Raman scattering in niobium oxides [12], we propose that this peak is due to Nb₂O₅ (and not NbO₂). In the bottom spectrum of figure 3, we also observed bands (off scale in the figure) at 620, 670 and 820 cm⁻¹, also consistent with this assignment [12]. Surprisingly, the oxide peaks are not observed in thicker flakes, suggesting either that the reaction may be taking place with the SiO₂ substrate rather than at the top surface, or that a reduced thermal conductivity in thin layers may make them more prone to oxidation. Another strong Raman band of Nb₂O₅ is expected to be seen at 996 cm⁻¹ but is masked in our case by the second order Si Raman band; on other substrates, this mode could be a useful diagnostic indicator of oxidation. In summary, our observations suggest that the physical damage due to laser exposure is probably due to photo-oxidation and is more pronounced in very thin flakes. Since Nb₂O₅ also shows strong Raman bands at 240 and 264 cm⁻¹ [12] which overlap the E_{2g} mode of NbSe₂, it is not surprising that the E_{2g} mode will appear to move non-monotonically with layer thickness whenever oxide formation occurs.

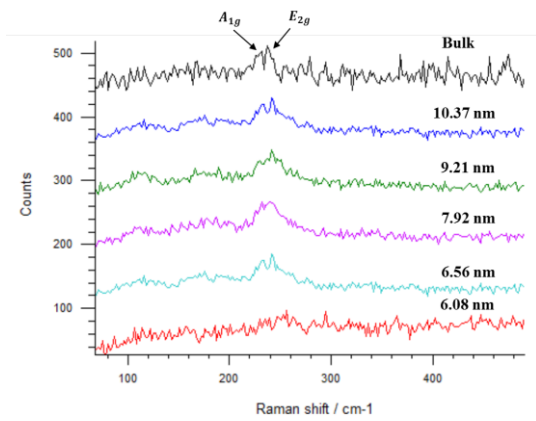


Figure 2. (Colour online) Raman spectra as a function of flake thickness captured with a laser power of 0.05 mW and an integration time of 100 s.

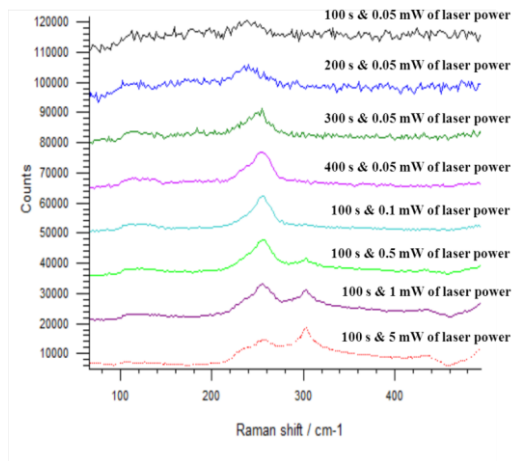


Figure 3. (Colour online) Series of Raman spectra for the same 6.56 nm thick NbSe₂ flake as a function of integration time and laser power illustrating the evolution of a new peak near 302 cm⁻¹.

3.2 Electrical and magnetotransport measurements

Systematic electrical measurements as a function of temperature, back-gate voltage and applied magnetic field were successfully performed on four NbSe₂ FETs with flake thicknesses in the range 6.56-10.37 nm. Room temperature sheet resistances, R_{sq} , reduced resistance ratios, RRR , and bulk resistivities, ρ_{Bulk} , for the four devices are summarized in table 1. Figure 4 plots the 300 K sheet resistances as a function of inverse thickness. We see that results for three of the devices are quite consistent, but the fourth falls well out of line with these. The dashed trend line on this graph represents

a much higher bulk resistivity by a factor of nearly seven than was assumed in earlier work on NbSe₂ by Frindt [7] (lower solid line). Very thin NbSe₂ flakes (1-2 unit cell flakes) appeared to be insulating, even though the end-to-end electrode resistances were less than 100 Ω. We speculate that the same reaction processes that occur under intense laser light may happen naturally during device processing, hence each device may have one or more 'dead' molecular layers and the thickness may not be a good measure of the number of electrically conductive layers. In contrast four point measurements at temperatures down to ~ 2 K on thicker flakes exhibited true zero resistance, as can be seen in figure 5 for a 9.21nm device. The inset of this figure shows an expanded view of the low temperature resistance data along with its digital derivative, dR/dT , whose smooth dependence indicates the absence of the charge density wave (CDW) transition observed in very high quality samples near $T=32\text{K}$ [13-15]. This was expected for our relatively low mobility NbSe₂ samples since it is known that an $RRR \sim 30$ or higher is needed to observe a CDW [16].

Table 1. Flake dimensions, sheet resistance, R_{squ} , bulk resistivity, ρ_{Bulk} , and reduced resistance ratio, RRR , for the four devices studied in detail.

Device thickness (d nm)	Flake width (W μm)	Flake length (L μm)	R_{squ} (Ω) at 300 K	ρ_{Bulk} (Ω.cm) at 300 K × 10 ⁻⁴	RRR
6.56±0.38	5.47±0.48	1.66±0.13	1400±0.36	9.20±0.14	---
7.92±0.32	1.56±0.08	2.17±0.22	690±0.18	5.44±0.06	5.27±0.18
9.21±0.35	2.89±0.24	1.34±0.13	1330±0.15	12.2±0.05	5.08±0.12
10.37±0.34	0.70±0.06	1.73±0.19	1170±0.02	12.1±0.1	4.62±0.19

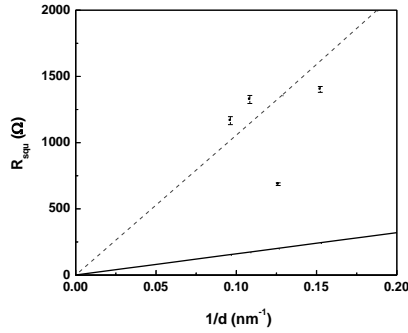


Figure 4. Sheet resistance as a function of inverse flake thickness for several devices. The solid black line represents values estimated from the bulk resistivity of large single crystals ($\rho_{bulk} = 160 \mu\Omega.cm$) [7].

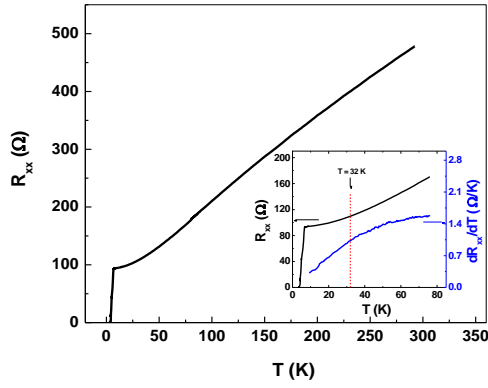


Figure 5. (Colour online) R_{xx} as a function of temperature for the 9.21 nm thick sample. The inset shows an expanded view of the low temperature data and its first derivative confirming the absence of a resistive signature of the CDW transition in this sample.

A careful analysis of the temperature dependent resistance $R_{xx}(T)$ of the 9.21 nm thick device was performed by making power law fits ($\sim T^n$) in the temperature ranges 10-40 K and 100-300 K as illustrated in figure 6. A good linear fit has been obtained in the 100-300 K range with $R_{xx} \sim T$, which is in agreement with predictions for a normal metal at temperatures above the Debye temperature Θ (calculated theoretically for NbSe₂ to be $\Theta \approx 190$ K [17]). In the range 10-40 K the dependence changed to $R_{xx} \sim T^2$, which can be attributed to electron-electron scattering according to Matthiessen's rule [18].

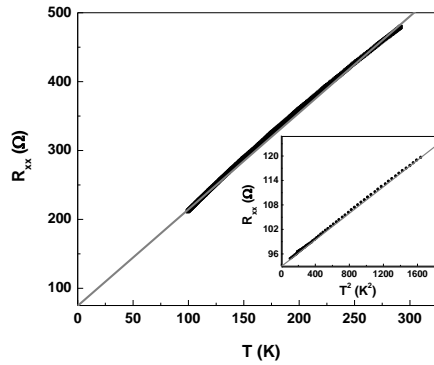


Figure 6. Linear fit obtained assuming $R_{xx} \sim T$ in the 100-300 K temperature range. Inset shows the fit to $R_{xx} \sim T^2$ in the 10-40 K temperature range.

Figure 7 shows an expanded view of a typical superconducting resistive transition which reveals signatures of multiple critical temperatures. Indeed all conducting flakes appeared to show at least two resistive transitions, some three. Note that AFM scans indicate that the flakes have a uniform thickness throughout the current-carrying region. Thus, we [believe/speculate](#) that these multiple resistive transitions are related to disorder in the layer stacking rather than lateral inhomogeneity as was proposed by Frindt [7] as an explanation for similar multiple transitions in his samples. Table 2 shows estimates of the multiple critical temperatures for all samples.

Table 2. A summary of the resistive transitions T_{c1} , T_{c2} and T_{c3} , and the mean field pairing temperature, T_{c0} , estimated from fits to the fluctuation conductivity above T_{c1} .

FET flake thickness (nm)	$T_{c1}(K)$	$T_{c2}(K)$	$T_{c3}(K)$	$T_{c0}(K)$
6.56 ± 0.38	6.14 ± 0.04	5.27 ± 0.06	---	6.40 ± 0.01
7.92 ± 0.32	6.35 ± 0.09	5.40 ± 0.06	4.99 ± 0.03	6.47 ± 0.01
9.21 ± 0.35	6.50 ± 0.07	5.06 ± 0.08	---	6.55 ± 0.02
10.37 ± 0.34	6.65 ± 0.06	5.43 ± 0.09	4.79 ± 0.12	6.67 ± 0.01

The highest temperature transition, T_{c1} , reduces monotonically as the flake thickness is reduced, but the low temperature transitions do not appear to vary particularly systematically. This can be clearly seen in figure 8, where both T_{c1} and T_{c2} are plotted as a function of flake thicknesses. It is interesting that all T_c s seem to extrapolate to approximately the same value at a thickness corresponding to one molecular layer of NbSe₂ ($d = 1\text{ML}$). [It is hence possible/This leads us to speculate](#) that the lowest T_c s [are/could possibly be attributed to associated with](#) single uncoupled NbSe₂ molecular layers. [This interpretation is in apparent conflict with the much lower estimates of the \$T_c\$ for 1ML flakes by Frindt \[7\] and Staley *et al.* \[5\]. However, it is not unreasonable that this discrepancy arises from very different disorder levels in the various experimental systems used.](#)

A linear suppression of T_c with decreasing thickness can be associated with enhanced Coulomb interactions and a reduction in electron screening arising from increasing disorder and interaction effects. Indeed a complete suppression of superconductivity and formation of an insulating state has been observed in highly disordered flakes [5, 7].

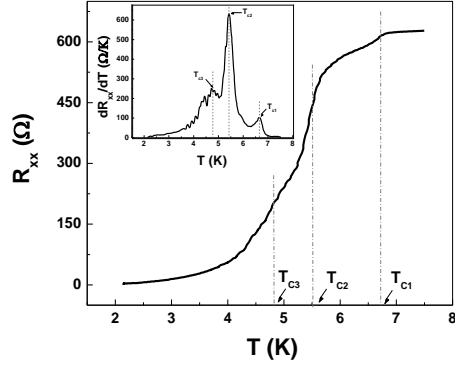


Figure 7. R_{xx} plotted as a function of temperature revealing three distinct superconducting transitions in a 10.37 nm thick device. Inset shows dR/dT which has been used to determine the T_c values.

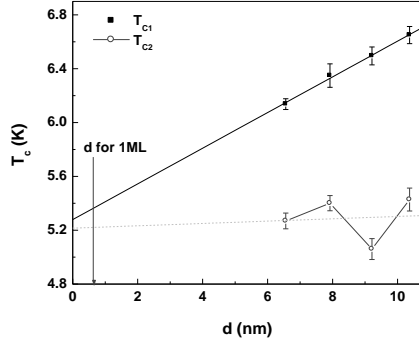


Figure 8. Measured values of resistive transitions T_{c1} and T_{c2} as a function of flake thickness.

3.2.2 Analysis of the $H=0$ resistive transition

A more detailed analysis of the $H = 0$ resistive transition has been made for all samples to extract both the mean-field pairing temperature, T_{c0} , from the fluctuation conductivity and, when possible, the Brezinskii-Kosterlitz-Thouless vortex-antivortex unbinding temperature, T_{BKT} . The onset T_{c0} values have been estimated by fitting the resistance data above T_{c1} to the Aslamazov-Larkin expression for the fluctuation-enhanced conductivity in 2D samples, $\Delta\sigma(T) \propto \ln(T/T_{c0})^{-1}$ (c.f., figure 9 (a)) [19]. The estimated T_{c0} values for all samples are listed in table 2. Below T_{c0} it is well established that a loss of global phase coherence and dissipation due to a finite flux resistance occur as a result of the penetration of thermally excited vortices. However, a finite supercurrent can flow below the BKT transition temperature, T_{BKT} , as a consequence of the formation of bound vortex-antivortex

pairs due to the attractive interaction between oppositely oriented vortices. The universal form of the flux flow resistance, $R_{xx}(T) \propto \exp[b(T - T_{BKT})^{-1/2}]$, has been used to identify T_{BKT} in our samples. In this expression the constant b is a measure of the strength of the vortex-antivortex interaction [20, 21]. In practice the unbinding temperatures have been extracted by plotting $[1/R_{xx} \cdot dR_{xx}/dT]^{-2/3}$ versus T at low temperatures and associating the T -axis intercept with T_{BKT} (c.f., figure 9). While estimation of T_{BKT} in the 9.21 nm and 10.37 nm thick samples was straightforward, it could not be achieved reliably in the 6.56 nm and 7.92 nm thick samples due to the presence of a small zero temperature resistance arising from weak device non-ideality. It is noteworthy that one of these latter two samples shows quite a long low-temperature BKT 'tail' while the other does not. It suggests that otherwise similar samples can have very different properties due to different degrees of stacking order [4]. In this case one of the samples appears to behave much more two-dimensionally than the other.

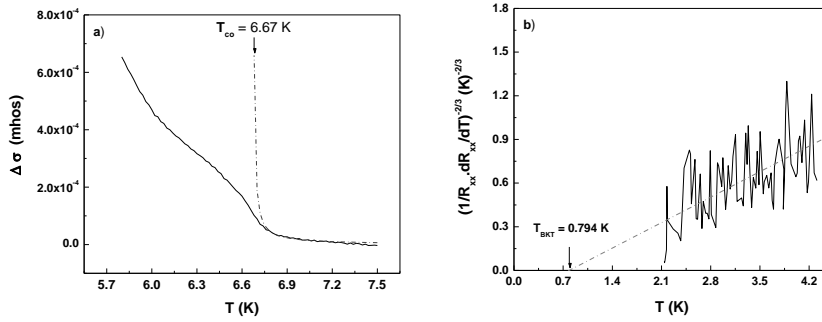


Figure 9. The mean field pairing temperature, T_{c0} , and the vortex-antivortex unbinding transition temperature, T_{BKT} , have been extracted using the Aslamazov-Larkin formula and the universal form of the flux flow resistance respectively for the 10.37 nm thick sample.

3.2.3 Resistive transition behavior as a function of applied magnetic field B

The temperature dependence of the resistance of the 9.21 nm thick sample at various values of magnetic field, B , and of the 10.37 nm device as a function of magnetic field at various values of temperature, T , are shown in figure 10. These data show how the resistive transitions tend to broaden and shift downwards in temperature with increasing magnetic field.

We assume that the upper critical field of high critical temperature superconducting 'pockets' controls the observed onset transition shift, whereas the shift in the tails near $R \sim 0$ can be attributed to vortex flow and the field dependence of the vortex-antivortex unbinding transition [22]. The field-dependent resistive transition temperatures have been estimated by determining the position of maximum slope from the first derivative of $R(T)$. The evolution of T_{c1} and T_{c2} as a function of applied magnetic field is plotted in figure 11(a) for the 9.21 nm thick sample. Plots of this type for each sample

allow us to calculate the zero-temperature upper critical field $H_{c2}(0)$ using the Werthamer-Helfand-Hohenberg (WHH) formula [23],

$$H_{c2}(0) = -0.69 T_c (dH_{c2}/dT)_{T=T_c}, \quad (1)$$

where T_c , is the resistive transition temperature and dH_{c2}/dT is the slope of $H_{c2}(T)$ at T_c .

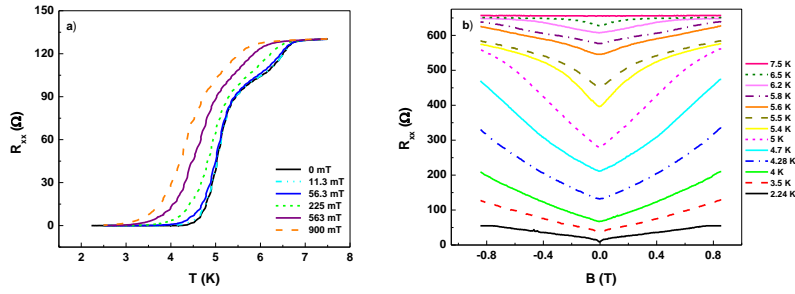


Figure 10. (Colour online) (a) Magnetic field dependence of $R(T)$ for a 9.21 nm thick sample. (b) Temperature dependence of $R(B)$ for a 10.37 nm thick sample.

A different estimation for $H_{c2}(0)$ can be made by using a phenomenological formula based on the Ginzburg-Landau equations for multiband superconductors [24],

$$H_{c2}(T) = H_{c2}(0)[1 - (T/T_c)^a]^b. \quad (2)$$

When $a = 1/0.69$ and $b = 1$ equations (1) and (2) become mutually consistent, and a good match between estimated values of $H_{c2}(0)$ can be obtained. Taking into account the fact that NbSe₂ is a multiband superconductor and $H_{c2}(T)$ is expected to be influenced by this, it is not clear *a priori* which of the two approaches is more appropriate. Figure 11 (b) shows fits made using equation (2) for both $T_{c1}(H)$ and $T_{c2}(H)$ for the 9.21 nm thick sample. Knowledge of $H_{c2}(0)$ allows the zero temperature Ginzburg-Landau coherence length, $\xi(0)$, to be calculated from the well-known relationship [25],

$$H_{c2}(0) = \phi_0/2\pi\xi(0)^2, \quad (3)$$

where ϕ_0 is the superconducting flux quantum. Values calculated for $H_{c2}(0)$ and $\xi(0)$ are summarized in table 3, and are in reasonably good agreement with other literature values [24, 26].

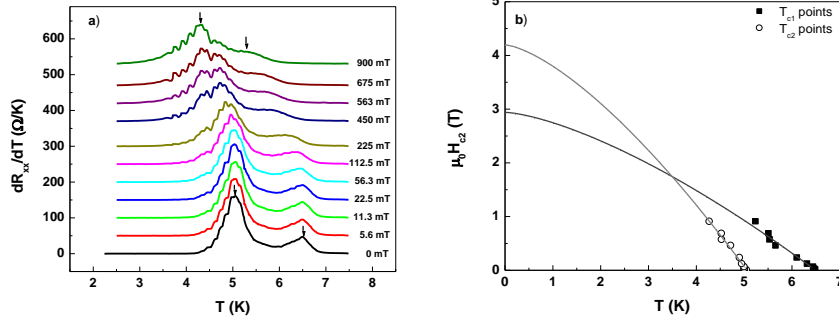


Figure 11. (Colour online) (a) Digital derivative of the $R(T, B)$ for a 9.21 nm thick sample showing the evolution of resistive transitions T_{c1} and T_{c2} . (b) Fits of equation 2 to $T_{c1}(H)$ and $T_{c2}(H)$ as estimated from (a)

Table 3. Table of the zero-temperature upper critical field, $H_{c2}(0)$, and G-L coherence length, $\xi(0)$, as estimated for three of the devices using equation 2

FET flake thickness (nm)	$H_{c2}(0)$ (T)		$\xi(0)$ (Å)	
	T_{c1}	T_{c2}	T_{c1}	T_{c2}
7.92 ± 0.32	3.30 ± 0.19	2.67 ± 0.18	98.2 ± 0.1	109.0 ± 0.1
9.21 ± 0.35	2.94 ± 0.14	4.2 ± 0.22	104.0 ± 0.1	87.1 ± 0.1
10.37 ± 0.34	3.93 ± 0.23	3.94 ± 0.26	90.0 ± 0.1	89.9 ± 0.1

3.2.4 The Influence of a back-gate voltage

Figure 12 shows the longitudinal conductivity, σ_{xx} , of the 10.37 nm thick sample as a function of V_g at $T = 7$ K. The data show an approximately linear *reduction* in conductivity with gate voltage, and the slope, $\Delta\sigma_{2D}/\Delta V_g$, allows one to calculate the dynamic field effect mobility, μ_{FE} , from [27],

$$\mu_{FE} = \frac{d}{\epsilon_r \epsilon_0} \frac{\Delta\sigma_{2D}}{\Delta V_g}, \quad (4)$$

where d is the SiO_2 layer thickness, ϵ_r is the relative dielectric constant of SiO_2 ($\epsilon_r = 3.9$) and ϵ_0 is the permittivity of free space. This rather indirect way to estimate the mobility of our devices is valuable since they have not been fabricated in a Hall bar configuration. The calculated dynamic mobilities μ_{FE} for our devices lie in the range of 7-64 cm^2/Vs at 7K, which is in agreement with the findings of Staley

et al. [5] but many orders of magnitude higher than values reported by Novoselov *et al.* [9]. Moreover, the observation that the conductivity *decreases* at positive gate voltages is in conflict with these latter results.

Finally we have investigated the influence of applied gate voltages of -100V and +100V on the resistive transition of samples. We observe a weak *reduction* in the resistive transition temperatures with more positive gate voltages. Figure 13 shows the digital derivative, dR/dT , of the temperature-dependent sheet resistance of a 10.37 nm thick sample at $V_g = -100$ V and $V_g = +100$ V in order to enhance the small shifts observed with gate voltage. The shift in T_c between these two values of V_g was estimated to be -10 mK and -45 mK for T_{c1} and T_{c2} respectively.

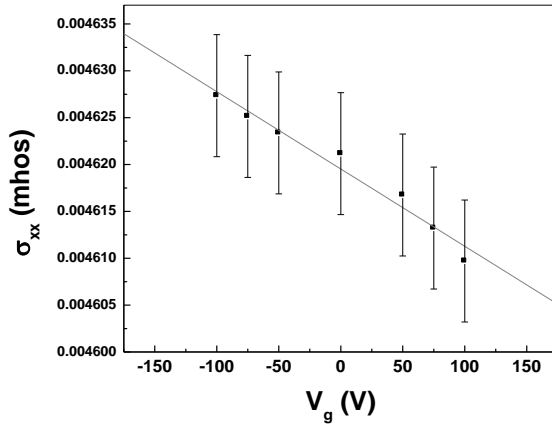


Figure 12. Plot of the longitudinal conductivity as a function of applied gate voltage, V_g , for a 10.37 nm thick sample at $T = 7$ K.

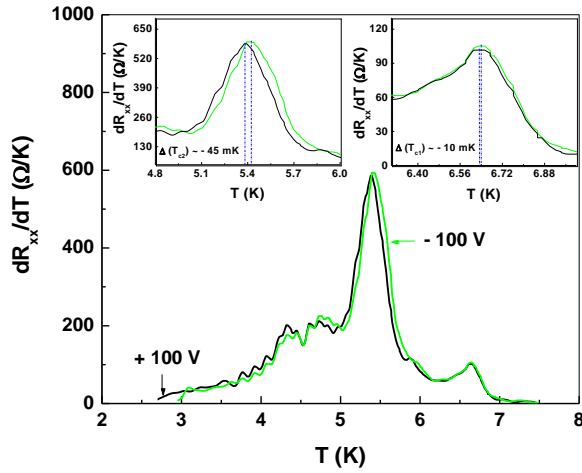


Figure 13. (Colour online) Plots of dR_{xx}/dT versus temperature showing the influence of a back gate voltage on the resistive superconducting transition of the 10.37 nm thick sample. Insets show expanded views of the changes around T_{c1} and T_{c2} .

4. Discussion

Patterning 4-terminal transport structures allows almost ideal measurements in which the influence of contact resistances is almost entirely eliminated. This distinguishes our results from the two-terminal measurements obtained by Staley *et al.* [5], who made 2-terminal measurements, while Frindt [7] does not actually state how measurements were made. Frindt [7] was not able to measure flake thickness directly but inferred it from the 300 K resistance assuming a bulk resistivity of $160 \mu\Omega\text{cm}$. Moreover However, we have made are able to directly measure the thicknesses of the our flakes and hence calculate an accurate value for the thicknesses and can correlate these with the 4-point device resistances. We measure an effective 300 K bulk resistivity for our samples that is seven times larger than typical values in single crystals suggesting that Frindt's values for flake thicknesses and resistivity may possibly have been considerably underestimated. One potential drawback of the use of lithographic patterning techniques is that it may possibility that it leads to the introduction of strain and stacking disorder. We note that Staley *et al.* [5] did not report multiple resistive transitions in their shadow masked two-terminal devices produced by less invasive shadow masking, although the superconducting transitions they show in their paper do appear to be relatively broad.

The resistive superconducting transition temperatures and their dependence on perpendicular magnetic field and back gate voltage have been studied as a function of NbSe₂ flake thickness to extend our current understanding of the underlying physics. The physical properties of highly anisotropic

~~systems such as NbSe₂ are strongly related to their crystal structure.~~ The three most common polytypes of ~~niobium diselenide this compound~~ are 2H-NbSe₂, 4H-NbSe₂, and 3R-NbSe₂. The first two hexagonal structures exhibit superconductivity below 7.2 K and 6.3 K respectively. In contrast the third rhombohedral structure is not superconducting down to 1.2K [28]. This illustrates rather graphically that the critical temperature of NbSe₂ depends very strongly on quite subtle changes in layer stacking. BCS theory tells us that this dependence can arise from both the density of electronic states near the Fermi energy and the phonon spectrum via the electron-phonon coupling strength. It is well established that the former depends quite strongly on the number of molecular layers [29, 30] as well as their stacking. Likewise the phonon spectrum is also known to depend on the number of layers [30], in particular the low frequency breathing and shear modes [31]. **The observed multiple resistive transitions must arise from lateral material inhomogeneities; if we had only vertical inhomogeneities down through the ML stack the low T_c regions would be shorted by the highest T_c region and only one transition would be observed.** ~~resistance of all our samples showed a small, sharp high temperature transition followed by one or more broader transitions which usually ended in a wide tail to zero resistance at low temperatures.~~ We speculate that the relatively large **amplitude** low temperature resistive transitions arise from quite large regions with different stacking order or strain, induced during mechanical exfoliation or lithographic processing. Only the small **amplitude** high temperature resistive transition shifts systematically downwards in thinner flakes. ~~consistent.~~ ~~This we tentatively attribute to with the the~~ **expected** dependence of density of **electronic** states and phonon spectrum on number of ML combined with enhanced Coulomb interactions and a reduction in electron screening arising from increasing disorder and interaction effects ~~in thinner samples.~~ The systematic linear dependence of T_{c1} on thickness suggests that it is a local property of all coupled molecular layers in the flake, possibly arising from small, well-separated pockets of superconductivity in a normal matrix. Such non-uniformities could be the consequence of disorder due to extrinsic charges in the adjacent SiO₂ dielectric or adsorbed molecules on the surface of the flake (c.f., the formation of electron/hole puddles in graphene [32]). ~~It is striking that T_{c1} and T_{c2} seem to extrapolate to approximately the same value near $d=1$ ML in figure 8. One possible interpretation of this is that the low T_c s relate to sections of single molecular layers that are almost completely uncoupled from the rest of the flake. This interpretation is in apparent conflict with the much lower estimates of the T_c for 1ML flakes by Frindt [7] and Staley *et al.* [5]. However, it is not unreasonable that this discrepancy arises from very different disorder levels in the various experimental systems used.~~

The lowest temperature transitions seem to be truly two-dimensional in nature with resistive tails dominated by the BKT vortex-antivortex unbinding transition. Normally the suppression of T_{BKT} well below the mean field transition temperature, as is the case in most of our samples, is only observed in highly disordered thin films with very short mean free paths. Simple estimates of the sheet resistance for a single NbSe₂ ML indicate that we are not in this limit. However, it is known that the attractive

Formatted: Highlight

Formatted: Font: Italic, Highlight

Formatted: Font: Italic, Subscript, Highlight

Formatted: Highlight

Formatted: Font: Italic, Highlight

Formatted: Font: Italic, Subscript, Highlight

Formatted: Highlight

vortex-antivortex interaction in 2D superconductors can be substantially screened through a material-dependent dielectric constant, ϵ_v , that linearly scales down T_{BKT} ($T_{BKT} \propto 1/\epsilon_v$) [33]. Hence the low value of T_{BKT} observed in most of our flakes suggests a relatively large screening parameter, ϵ_v , leading to weakly bound vortices and antivortices.

The evolution of different resistive transitions has been tracked as a function of applied perpendicular magnetic field allowing values of the zero temperature upper critical field, $H_{c2}(0)$, and GL coherence length, $\xi(0)$, to be independently estimated. Fits of WHH theory to $H_{c2}(T)$ for the different resistive transitions reveals quite a large scatter in $H_{c2}(0)$ and $\xi(0)$ with no systematic variation as a function of flake thickness. The measured $T=0$ critical fields of $\sim 3 - 4$ T are considerably lower than typical values for bulk single crystals ($H_{c2}(0) \sim 14.6$ T [26]), partly due to the reduced critical temperatures for our flakes. Surprisingly the estimated coherence lengths of $\sim 9 - 11$ nm are slightly larger than those measured in single crystals ($\xi(0) \sim 7.7$ nm [26]). This is not what one would expect since the high levels of disorder in our flakes should lead to a significant reduction in $\xi(0)$. For example, if we assume our samples are in the dirty limit ($l \ll \xi$), where l is the electron mean free path, one expects the zero temperature GL coherence length to be reduced to $\xi(0) = 0.85(\xi_0 l)^{1/2}$ [25], where ξ_0 is the BCS coherence length.

The decrease of normal state conductance and resistive transition temperatures were found to depend weakly on the back gate voltage with both conductivity and T_c decreasing as the with increased electron concentration is consistent with is increased. Recent pseudopotential DFT calculations of the electronic density of states in few molecular layer 2H-NbSe₂ [29]. These predict that it exhibits a sharp peak about 100 meV below the Fermi energy and a strong downward slope as it crosses E_F . This calculated falling density of states with increasing electron concentration is fully consistent with the measured reduction in the conductivity at positive back gate voltages. Also, since the applications of a gate voltage would not be expected to significantly change the phonon spectrum or electron-phonon coupling, a reduction in density of electronic states would also account for the observed reduction in T_c . The fact that it is noteworthy that the low temperature transitions shift more than four times faster with gate voltage than the small high temperature transition indicates that the former are associated with. This suggests that the former have active regions composed of fewer molecular layers that possibly also lie layers that lie closer to the SiO₂ gate dielectric where electric fields are strongest.

Our studies of superconductivity in NbSe₂ flakes have thrown up many questions that merit further investigation. Future work will focus on improving the electronic properties (e.g., mobility, carrier concentration, back-gate efficiency) of 2H-NbSe₂ flakes. In particular, it appears that the act of patterning contacts may be enough to create strain in the flakes and induce layer stacking disorder. Hence, it would be interesting to compare devices prepared with a lithography-free technique, e.g., such as the shadow masking as used approach reported by Staley *et al.* [5], which to pattern contacts

Formatted: Subscript

~~as this~~ could yield higher mobilities and lower levels of strain. Exfoliation onto a different substrate such as CVD h-BN should also greatly reduce levels of disorder arising from extrinsic charges in the SiO₂ dielectric. ~~Alternatively, lowering the device processing temperatures, as well as sonication powers used during cleaning and lift off, should lead to less damage during lithography based fabrication.~~ The ability to apply larger electric fields will also lead to much larger shifts in T_c and replacing SiO₂ by a higher permittivity gate dielectric, e.g., HfO₂, could enhance FET performance as demonstrated by Zhang *et al.* [34] in ~~their~~ ambipolar MoS₂ FETs. Finally, accurate calculations of the electronic band structure (and DOS), phonon spectrum and electron-phonon coupling in NbSe₂ flakes with different layer stacking orders are urgently required to inform experimental work. These theoretical studies will need to be complemented by detailed structural characterisation of our samples (e.g., by STM/STS or HRTEM) in order to obtain a systematic understanding of the behaviours we have observed.

5. Conclusions

In conclusion, systematic investigations of superconductivity in few molecular layer NbSe₂ flakes have been performed in well-characterised 4-terminal devices. ~~Quite large flakes were~~ produced by mechanical exfoliation from a 2H-NbSe₂ single crystal onto Si/SiO₂ substrates ~~and could be readily identified under an optical microscope.~~ While devices fabricated from extremely thin NbSe₂ flakes did not appear to conduct, slightly thicker flakes were superconducting with an onset T_c that was only slightly depressed from the bulk value. All devices exhibited multiple resistive transitions, even though AFM scans confirmed that flakes were of uniform thickness. We attribute this to local regions of strain and layer stacking disorder in our samples. The application of a positive back gate voltage (increased electron density) led to a weak reduction in conductivity and critical temperature consistent with ~~recent calculations of the electronic~~ ~~the predicted downward slope of the~~ density of states ~~near the Fermi energy.~~ Measurements of ~~$H_{c2}(T)$ the temperature dependent upper critical~~ field reveal that $H_{c2}(0)$ is strongly suppressed while surprisingly $\xi(0)$ is significantly increased with respect to typical values for bulk 2H-NbSe₂. A complete understanding of the observed phenomena will require careful characterization of the stacking order in our samples combined with a detailed theoretical analysis of the band structure, phonon spectrum and electron-phonon coupling of realistic NbSe₂ flakes. ~~We hope that~~ This work ~~should~~ ~~will~~ inform investigations of other 2D superconducting crystals in common layered materials ~~such as Bi₂Sr₂CaCu₂O_{8+x},~~ allowing the exploration of new physics and possible device applications.

6. Acknowledgements

The authors acknowledge financial support from the Egyptian government and Ain Shams University, EPSRC in the UK under grant nos. EP/G036101/1 and the NanoSC COST Action MP-1201. We are grateful to ~~Prof. D McK Paul and Prof. G. Balakrishnan Dr C.D. Dewhurst~~ (University of

Formatted: Font: Italic

Formatted: Font: Italic, Subscript

Formatted: Font: Italic

Formatted: English (United States)

[WarwickInstitut Laue-Langevin, Grenoble](#)) for providing a high quality 2H-NbSe₂ single crystal for [this work](#) exfoliation. SR acknowledges financial support from EPSRC grant no. EP/K010050/1

References

- [1] Novoselov K, Geim A K, Morozov S, Jiang D, Zhang Y, Dubonos S, Grigorieva I and Firsov A 2004 Electric field effect in atomically thin carbon films *Science* **306** 666-9
- [2] Coleman J N, Lotya M, O'Neill A, Bergin S D, King P J, Khan U, Young K, Gaucher A, De S, Smith R J, Shvets I V, Arora S K, Stanton G, Kim H Y, Lee K, Kim G T, Duesberg G S, Hallam T, Boland J J, Wang J J, Donegan J F, Grunlan J C, Moriarty G, Shmeliov A, Nicholls R J, Perkins J M, Grievson E M, Theuwissen K, McComb D W, Nellist P D and Nicolosi V 2011 Two-Dimensional Nanosheets Produced by Liquid Exfoliation of Layered Materials *Science* **331** 568-71
- [3] Benameur M, Radisavljevic B, Heron J, Sahoo S, Berger H and Kis A 2011 Visibility of dichalcogenide nanolayers *Nanotechnology* **22** 125706
- [4] Mattheis L F 1973 Band structures of transition-metal-dichalcogenide layer compounds. *Physical Review B* **8** 3719-40
- [5] Staley N E, Wu J, Eklund P, Liu Y, Li L J and Xu Z 2009 Electric field effect on superconductivity in atomically thin flakes of NbSe₂. *Physical Review B* **80**
- [6] Wang Q H, Kalantar-Zadeh K, Kis A, Coleman J N and Strano M S 2012 Electronics and optoelectronics of two-dimensional transition metal dichalcogenides *Nature Nanotechnology* **7** 699-712
- [7] Frindt R F 1972 Superconductivity in Ultrathin NbSe₂ layers *Physical Review Letters* **28** 299-301
- [8] Borisenko S V, Kordyuk A A, Yaresko A N, Zabolotnyy V B, Inosov D S, Schuster R, Buchner B, Weber R, Follath R, Patthey L and Berger H 2008 Pseudogap and charge density waves in two dimensions *Physical Review Letters* **100**
- [9] Novoselov K S, Jiang D, Schedin F, Booth T J, Khotkevich V V, Morozov S V and Geim A K 2005 Two-dimensional atomic crystals *Proceedings of the National Academy of Sciences of the United States of America* **102** 10451-3
- [10] Wu Y, An M, Xiong R, Shi J and Zhang Q 2008 Raman scattering spectra in the normal phase of 2H-NbSe₂ *Journal of Physics D: Applied Physics* **41** 175408
- [11] Myers G and Montet G 1971 Light-induced oxidation of NbSe₂ single crystals *Journal of Physics and Chemistry of Solids* **32** 2645-6
- [12] Huang B X, Wang K, Church J S and Li Y-S 1999 Characterization of oxides on niobium by raman and infrared spectroscopy *Electrochimica Acta* **44** 2571-7
- [13] Corcoran R, Meeson P, Onuki Y, Probst P-A, Springford M, Takita K, Harima H, Guo G and Gyorffy B 1994 Quantum oscillations in the mixed state of the type II superconductor 2H-NbSe₂ *Journal of Physics: Condensed Matter* **6** 4479
- [14] Stiles J, Williams D L and Zuckermann M 1976 Dependence of the critical temperature for the formation of charge density waves in 2H-NbSe₂ upon impurity concentration *Journal of Physics C: Solid State Physics* **9** L489
- [15] Berthier C, Molinié P and Jérôme D 1976 Evidence for a connection between charge density waves and the pressure enhancement of superconductivity in 2H-NbSe₂ *Solid State Communications* **18** 1393-5
- [16] Iwaya K, Hanaguri T, Koizumi A, Takaki K, Maeda A and Kitazawa K 2003 Electronic state of NbSe₂ investigated by STM/STS *Physica B: Condensed Matter* **329** 1598-9
- [17] Naito M and Tanaka S 1982 Electrical transport properties in 2H-NbS₂, NbSe₂, TaS₂ and TaSe₂ *J. Phys. Soc. Jpn* **51** 219-27

- [18] Volkenshtein N, Dyakina V and Startsev V 1973 Scattering mechanisms of conduction electrons in transition metals at low temperatures *physica status solidi (b)* **57** 9-42
- [19] Aslamazo.Lg and Larkin A I 1968 Influence of fluctuation pairing of electrons on conductivity of normal metal. *Physics Letters A A* **26** 238-9
- [20] Minnhagen P 1987 The two-dimensional Coulomb gas, vortex unbinding, and superfluid-superconducting films. *Reviews of modern physics* **59** 1001-66
- [21] Kessler B M, Girit C O, Zettl A and Bouchiat V 2010 Tunable Superconducting Phase Transition in Metal-Decorated Graphene Sheets *Physical Review Letters* **104**
- [22] Zhu X, Yang H, Fang L, Mu G and Wen H-H 2008 Upper critical field, Hall effect and magnetoresistance in the iron-based layered superconductor $\text{LaFeAsO}_{0.9}\text{F}_{0.1-0.6}$ *Superconductor Science and Technology* **21** 105001
- [23] Werthamer N, Helfand E and Hohenberg P 1966 Temperature and Purity Dependence of the Superconducting Critical Field, H_{c2} . III. Electron Spin and Spin-Orbit Effects *Physical Review* **147** 295
- [24] Zehetmayer M and Weber H 2010 Experimental evidence for a two-band superconducting state of NbSe_2 single crystals *Physical Review B* **82** 014524
- [25] Tinkham M 2004 *Introduction to superconductivity* vol 1: Dover Publications)
- [26] Banerjee S, Patil N, Ghosh K, Saha S, Menon G, Ramakrishnan S, Grover A, Mishra P, Rao T and Ravikumar G 1997 Magnetic phase diagram of anisotropic superconductor 2H-NbSe_2 *Physica B: Condensed Matter* **237** 315-7
- [27] Staley N E, Puls C P and Liu Y 2008 Suppression of conductance fluctuation in weakly disordered mesoscopic graphene samples near the charge neutral point *Physical Review B* **77** 155429
- [28] Andreeva O, Braude I and Mamalui A 2012 Selenium vacancies and their effect on the fine structure of NbSe_2 quasi-two-dimensional single crystals *The Physics of Metals and Metallography* **113** 888-92
- [29] Lebègue S and Eriksson O 2009 Electronic structure of two-dimensional crystals from ab initio theory *Physical Review B* **79**
- [30] Calandra M, Mazin I and Mauri F 2009 Effect of dimensionality on the charge-density wave in few-layer 2H-NbSe_2 *Physical Review B* **80** 241108
- [31] Molina-Sánchez A and Wirtz L 2011 Phonons in single-layer and few-layer MoS_2 and WS_2 *Physical Review B* **84** 155413
- [32] Allain A, Han Z and Bouchiat V 2012 Electrical control of the superconducting-to-insulating transition in graphene-metal hybrids *Nature materials* **11** 590-4
- [33] Epstein K, Goldman A and Kadin A 1982 Renormalization effects near the vortex-unbinding transition of two-dimensional superconductors *Physical Review B* **26** 3950
- [34] Zhang Y, Ye J, Matsushashi Y and Iwasa Y 2012 Ambipolar MoS_2 Thin Flake Transistors. *Nano letters* **12** 1136-40

